CrossMark

RESEARCH PAPER

Micro-optofluidic switch realized by 3D printing technology

Fabiana Cairone[1] · Salvina Gagliano[1] · Domenico C. Carbone[2] · Giuseppe Recca[2] ·
Maide Bucolo[1]

Abstract This paper presents a PDMS micro-optofluidic chip that allows a laser beam to be driven directly toward a two-phase flow stream in a micro-channel while at the same time automatically, detecting the slug's passage and stirring the laser light, without the use of any external optical devices. When the laser beam interacts with the microfluidic flow, depending on the fluid in the channel and the laser angle of incidence, a different signal level is detected. So a continuous air–water segmented flow will generate a signal that switches between two values. The device consists of a T-junction, which generates the two-phase flow, and three optical fiber insertions, which drive the input laser beam toward a selected area of the micro-channel and detects the flow stream. Three micro-channel sections of different widths were considered: 130, 250, 420 µm and the performance of the models was obtained by comparing ray-tracing simulations. The master of the device has been realized by 3D printing technology and a protocol which realizes the PDMS chip is presented. The static and dynamic characterizations, considering both single flows and two-phase flows, were carried out, and in spite of the device's design simplicity, the sensitivity of the system to capture changes in the segmented flows and to stir the laser light in different directions was fully confirmed. The experimental tests show the possibility of obtaining satisfactory results with channel diameters in the order of 200 µm.

1 Introduction

The lack of an active control over individual drops severely limits the use of the micro-system for microfluidic application (Baroud et al. 2007a). Acting on individual drops in micro-channels is still a challenge. The body force scales with the cube of the drop radius, so at small scales, it is natural to look for surface mechanisms for the droplet manipulation (Tabeling 2005). In this context for chemical and biochemical applications, optical techniques are acquiring a central role in representing a good solution in both control and sensing processes (Whitesides 2006; Yeshaiahu et al. 2010).

Regarding the control, recent works have demonstrated that the force near to the µN range could be produced on a droplet interface with a laser wave to control its displacement (Baroud et al. 2007b). The theoretical analysis for localized heating shows that force scaling is highly favorable to miniaturization, since the total force is predicted to increase as the drop radius decreases. On the other hand, the most common way to investigate the microfluidic flows is by continuous 2D monitoring using a fast CCD camera or a PIV system allowing to discern emulsions and flow with heterogeneous cross section (Van Steijn et al. 2007) with the drawbacks related to costly and bulky equipments. In the case of flow segments that occupy the entire cross-section a simplified signal monitoring setup is possible by using photodetectors (Schembri and Bucolo 2011) coupled with micro-optical components.

During the last decade soft-lithography technology has allowed the rapid prototyping of the micro-optofluidics device using polydimethylsiloxane (PDMS) (Ng et al.

✉ Maide Bucolo
maide.bucolo@dieei.unict.it

1 Dipartimento di Ingegneria Elettrica Elettronica e Informatica, University of Catania, viale A.Doria 6, 95125 Catania, Italy

2 CNR National Research Council of Italy - IPCB Institute for Polymers, Composites and Biomaterials, Via Gaifami 18, 95126 Catania, Italy

2002; McDonald and Whitesides 2002), a polymer that is well-known for its high chemical resistance, biological compatibility, as well as, for its good optical properties and versatility in the realization of micro-optical components. Examples of the PDMS technology in the miniaturization of micro-optic components are reported in literature such as waveguide (Chang-Yen et al. 2005), mirrors (Llobera et al. 2008) and lenses (Camou et al. 2003) and are already used in applications (Ono et al. 2003; Llobera et al. 2007). Previous works provide the versatility of micro-optical interfaces based on PDMS waveguide, micro-lenses and micro-mirrors in focusing and detecting the light information for point-wise flow monitoring, both in vivo (Sapuppo et al. 2010) and in vitro (Sapuppo et al. 2012) contexts, being an alternative to standard microscopy and integrated velocimetry (Sapuppo 2007) optical methods.

All these aspects were taken into account in the realization of the presented PDMS micro-optofluidic device allowing a laser beam to be driven directly toward a two-phase flow stream in the micro-channel while, at the same time, detecting the slug's passage and stirring the laser beam, without the use of any external optical devices. When the laser beam interacts with the microfluidic flow, depending on the fluids in the channel and the laser angle of incidence, a different signal level can be detected. So a continuous air–water segmented flow will generate a signal that switches between two values. Furthermore this device has been realized by 3D printing technology and a protocol to realize the chip in PDMS is presented.

The theoretical background behind the device realization is the total internal reflection occurring at a boundary between two media, when the incident angle of a source light beam is greater than the critical angle related to the media refractive indexes. The same principle is applied (Rossetto and Ferrante 2014) by using an external and more complex optical setup, that involves the light alignment related to the reflection and refraction at several subsequent boundaries. The embedding of the optical fiber insertions in the chip design has allowed a reduction in the number of the interfaces crossed by the light and a satisfactory performance is achieved even without the use of lenses.

The variety of applications related to the use of this class of embedded micro-optofluidic devices is enormous. Two examples based on single-flow monitoring are described in Weber et al. (2012) and Lapsley et al. (2009). In the first a micro-optofluidic device was used to determine the concentration of lactose in a liquid. In the latter, a variable optical attenuator device is obtained by altering the refractive index of the fluid within the micro-channel.

Recently, 3D printing technology has spread across many disciplines (Hwanga et al. 2015). An innovative aspect discussed in this paper is its use in the fabrication of the micro-optofluidic mold. In most of the works in this field, as the pneumatically tunable optofluidic switch realized in Song and Psaltis (2011), the mold is realized by standard soft-lithography. Although 3D printed structures cannot currently compete with the resolution of structures defined using soft-lithography, several advantages can be foreseen such as the simplification in the fabrication of structures with different heights or suspensions and the diversification of the chip's materials (no longer limited by the 3D printable resins) (Chan et al. 2015). Thanks to its design flexibility, it would be possible to create channels quickly and inexpensively with unprecedented complexity, as well as integrating micro-optic components.

In Sect. 2, initially the theoretical background behind the design of the micro-optofluidic switch will be presented. Then the chip design, considering the three micro-channel widths of 130, 250, 420 μm, will be described in detail comparing the performance of the models obtained by ray-tracing simulations. Following in the same section, the protocol used for the 3D printing realization and the characteristics of the mold and PDMS device realized will be presented. Finally in Sect. 3, the experimental results obtained during the static and dynamic characterizations of the devices will be discussed. In the static characterization, the optical power measurements were carried out to evaluate the performance of the device as a laser stirrer and its losses in single-flow conditions. In the dynamic characterization, the attention was focused on the generation and description of the switch signals obtained during the two-phase flow.

2 Embedded system design and realization

2.1 Theoretical background

In this micro-optofluidic switch design the choice of the material to realize the chip and its geometry, as well as, the choice of the fluids for the two-phase flow generation played a fundamental role. The operative principle was considered as follows: assuming that two fluids with quite different refractive indexes flow in a microfluidic channel and an incident laser beam interferes with them in a test section, we can obtain a selective light reflection and transmission based on which fluid is interfering with the laser at that moment. This is possible in specific geometric conditions established in relation to the fluids and material refractive indexes. The polymer selected to realize the chip was the polydimethylsiloxane (PDMS), for its optical properties (refractive index $n_{PDMS} = 1.41$) and fast device prototyping (McDonald and Whitesides 2002). The fluids used to generate the two-phase flow were the air and deionized (DI) water that have the refractive indexes $n_{air} = 1$ and $n_{water} = 1.33$, respectively.

In Figs. 1 and 2 two graphic representations of the aforementioned working principle are shown: the reflection condition at the air passage along with the transmission condition at the water passage. Snell's law allows the computation of the limit angles for the total reflection at the interfaces PDMS\AIR ($\theta_{L_1} = 45.17°$) and PDMS\WATER ($\theta_{L_2} = 70.6°$). Considering a micro-channel test section and positioning a laser beam with an inclination angle (α) in relation to a micro-channel perpendicular in the range $\theta_{L_1} < \alpha < \theta_{L_2}$, the light will be reflected at the air passage (Fig. 1) and transmitted at the water passage (Fig. 2). Based on geometrical optics it is possible to compute the angles of the reflected and transmitted light beams. The reflection angle is the same as the incident angle α, while for the transmission angle, the light passage through two subsequent interfaces has to be considered: the PDMS\WATER and the WATER\PDMS. As it can be deduced by geometrical considerations in Fig. 3, the final inclination of the light path in relation to the channel perpendicular is the same
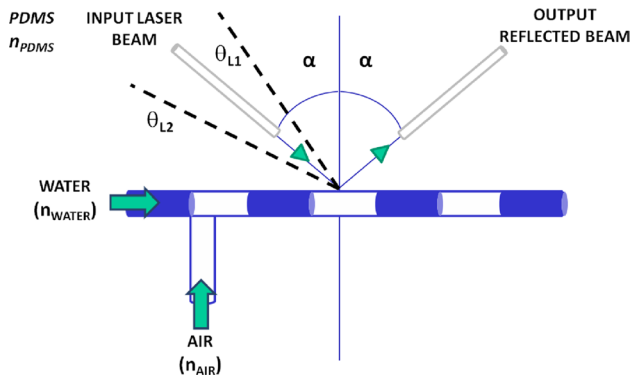

Fig. 3 In the transmission condition, the input beam crosses both micro-channel walls and a beam displacement (d) is induced by the double light refraction

(α), but the double light refraction induces a beam displacement (d) depending on the channel dimension (h) and the medium refractive indexes at the interface, as in Eq. 1.

$$d = h \sin \alpha \left(1 - \frac{\cos \alpha}{\sqrt{\left(\frac{n_1}{n_2}\right)^2 - \sin^2 \alpha}} \right) \tag{1}$$

2.2 Design and simulations

The device computer-aided design (CAD) consists of a rectangular box with an internal area (85×40 mm); the micro-channel is at the center of the box and the sections for the fiber insertions are above and below. Three optical fiber insertions were designed: one is used to drive the input laser beam toward the channel and the other two to acquire the optical information related to the light reflected (OF_1) and transmitted (OF_2), as shown in Fig. 4.

The distance (D) between the micro-channel and the fiber insertions is 500 μm (see Fig. 5b). The width (w) of the micro-channel and the fiber insertions are equal while the height of the fiber insertions (z) were designed larger than the fiber cladding diameter for an easier placement (see Fig. 5a). Three device CADs were considered based on the cladding diameter of the used fibers: CAD_{400} with $w = 420$ μm, CAD_{200} with $w = 250$ μm and CAD_{100} with $w = 130$ μm.

The micro-channel has a squared section, the diameter of the inlet and outlet wells is 2.4 mm. The T-junction is at a distance of 13 mm from the inlet wells. The total length

Fig. 1 The working principle representation in the reflection condition: the input laser beam with a specific inclination (α) points in a micro-channel test section during the air passage and the output light beam is reflected
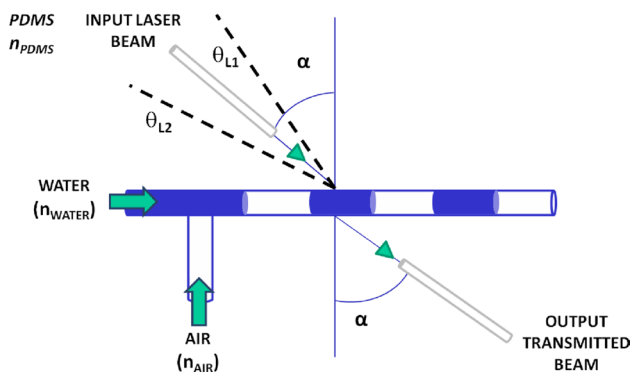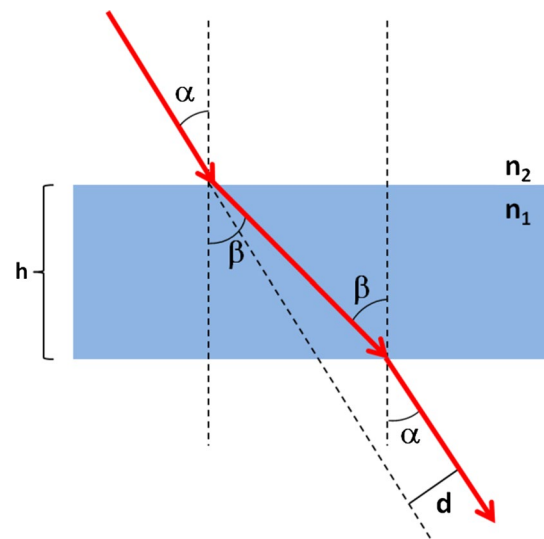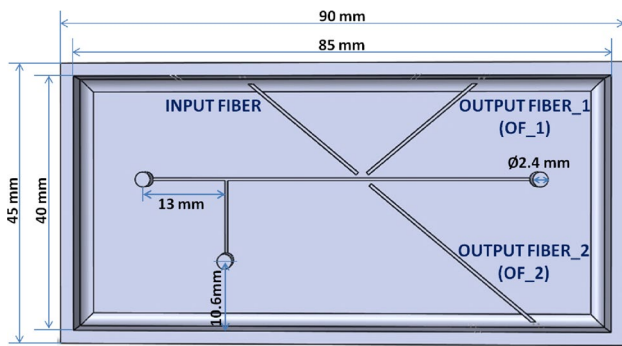

Fig. 2 The working principle representation in the transmission condition: the input laser beam with specific inclination (α) points in a micro-channel test section during the water passage and the output light beam is transmitted

Fig. 4 The CAD representation and measurements in a frontal perspective: the microfluidics T-junction and the optical fiber insertions. The input fiber insertion is for the optical fiber to be connected with the laser, the output fiber_1 and output fiber_2 are for the fibers that collect the light reflected (OF$_1$) and the light transmitted (OF$_2$) during the two-phase flow passage
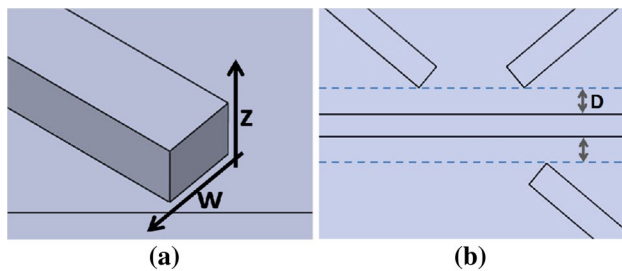

Fig. 5 Focusing on the CAD. **a** The rectangular section of the fiber insertions. **b** The micro-channel test section at the center with the three fiber insertions above and below

Fig. 6 The laser source model designed to reproduce the fiber N.A. = 0.22 and the light dispersion along the channel surface (L)

Table 1 Characteristics of the three device CADs (in μm): optical fiber cladding diameter (c), micro-channel and fiber insertions width (w), optical light displacement (d), and fiber insertions height (z)

	c	w	d	z
CAD$_{400}$	408	420	54.28	520
CAD$_{200}$	245	250	32.31	350
CAD$_{100}$	126	130	16.80	230

Table 2 Characteristics of the optical fiber model used in the three device CADs

	AO (μm)	AH (μm)	OH (μm)	L (mm)
CAD$_{400}$	182.5	184.76	28.84	1.00
CAD$_{200}$	100.0	101.24	15.80	0.78
CAD$_{100}$	52.5	53.15	8.31	0.59

of the channel from the junction to the outlet well is 46 mm and the test section is at the center.

The optical fibers used for the light acquisition were multi-mode with a N.A. = 0.22. To satisfy the working principle discussed in Sect. 2.1 the angle of the laser light input insertion (α) has to be in the range [45°, 70°]. The value $\alpha = 50°$ was selected to minimize the beam dispersion on the micro-channel (L) due to laser beam N.A. (see Fig. 6). The insertion for light reflected acquisition (OF$_1$), consequently, was set to $-\alpha$. On the opposed micro-channel side, the fiber insertion for the light transmitted acquisition (OF$_2$) is positioned with an inclination of α and a displacement (d) in relation to the input test section due to the translation of the input light beam crossing the micro-channel.

In Table 1, for each CAD, the cladding of the optical fibers considered (c), the relative micro-channel and fiber insertions width (w), the fiber insertions height (z) and, assuming the channel filled by water, the relative displacement of output fiber insertion (d) are summarized.
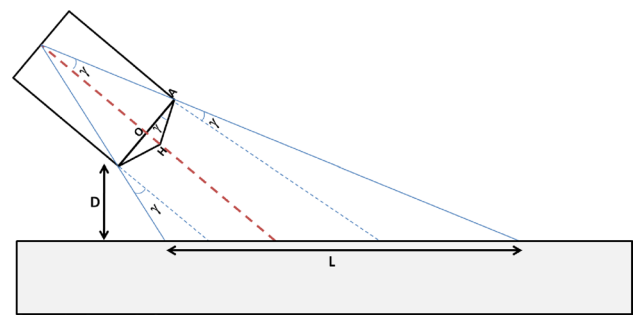
The performance of the device models were evaluated by ray-tracing simulations (software TracePro by Lambda Research Corporation). The laser source model designed to reproduce the fiber N.A. = 0.22 is reported in Fig. 6. The angle γ is 9° and by geometrical considerations, considering the optical fiber core radius (AO) associated with the different designed CADs, the lengths of OH and AH and the light dispersion along the channel surface (L) were computed and reported in Table 2.

In Fig. 7a, b, the ray-tracing results obtained in simulations for CAD$_{400}$ when the channel was filled respectively by air (in left column) and water (in right column) are plotted. Additionally in Fig. 7c, d, the spatial (2D) distributions of the rays at the test section are shown where the vertical solid lines mark the boundaries of the micro-channel surface. The number of incident rays is greater than the 95 % at both the air and water presence. Assuming that each ray has a specific energy, the total flux was computed around 0.94 mW with a loss of 6 %. Additionally,
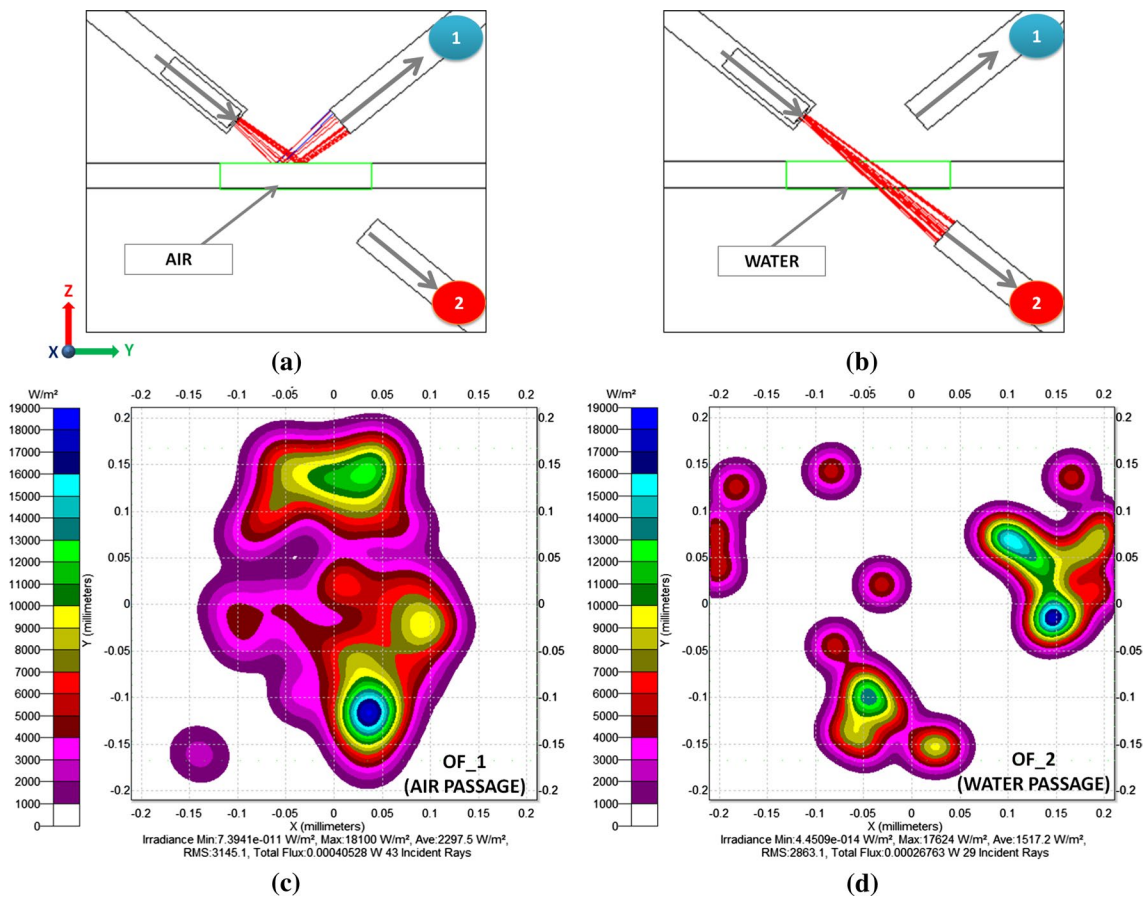
Fig. 7 The ray-tracing results obtained in simulations for CAD_{400} when the channel was filled respectively by air (in *left column*) and water (in *right column*): the plots in (**a**, **b**) are the rays paths; the plots in (**c**, **d**) are the spatial (2D) distributions of the rays at the test section

the percentage of rays incidental to the fiber OF_1 during the air passage and into the fiber OF_2 during the water passage are, each in order, 40 % with a total flux 0.39 mW (a total loss of 4 dB) and 25 % with a total flux 0.26 mW (a total loss of 6 dB). The decrease in the performance is caused by the dispersion of the rays L all along the channel test section (see Fig. 6) and by the thickness of PDMS layer that covers the chip. Considering three values {0.5; 1; 7} mm for the thickness of the PDMS cover layer, a comparative study for CAD_{400} was carried out. Although a greater thickness guarantees the robustness of the chip, it was verified that when a ray's dispersion of around 4 % per 0.1 mm is introduced for a thickness of up to 1 mm, then it changes slightly. A cover layer of 0.5 mm, was used as an optimal tradeoff.

The comparison of the CAD's performance is reported in Fig. 8. The bar-plot is related to the percentage of rays incidental to the surfaces of interest: the micro-channel test section (labelled as bubble surface) and the fiber OF_1 and OF_2 during the air and the water passage respectively. The color codes the considered CAD. As expected, a decrease in performance was evinced by reducing the channel and

fiber insertion width (w) and, because of this, the attention in the device realization was focused on CAD_{400} and CAD_{200}.

2.3 Fabrication process

The PDMS micro-optofluidic devices were realized by 3D-printing technology. The developed protocol consists of four steps: the CAD design of the master, the master realization by the 3D Printer (the mold), the surface treatment of the master and finally the PDMS chip realization (the slave).

The CAD of the master was designed in Solidworks, as described in detail in Sect. 2.2, and sent to the 3D Printer (Object 30). It has a resolution of 49 μm in the work plane and, of 28 μm along the z axis, that is the direction along which the printhead of the printer moves. The accuracy is around 0.1 mm with slight variations depending on the geometry, the size, the orientation, the material and the post-processing method. Two polymers are used by the printer: the Whiteplus 835 (inspired by ABS) is the main polymer and the FullCure 705 is the support polymer.
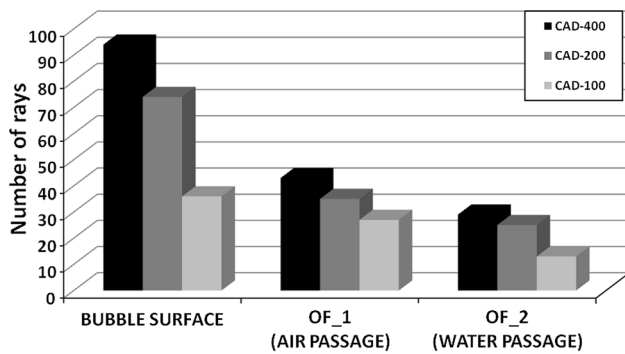
Fig. 8 Comparison of the performance considering the device CADs: CAD_{400}, CAD_{200} and CAD_{100}. The *bar-plot* reports the percentage of rays incidence on the surfaces of interest at the air and water passage

In the second step a thin layer of Sokalan, in a solution with a solvent, was deposited on the printed master to improve the affinity surface and to ensure an easy peeling of the PDMS slave from the mold. After depositing the Sokalan, the master was placed in oven at 50 °C for 5 min, because the Sokalan has to be perfectly dry so as not to compromise the next step of PDMS polymerization.

The two components of PDMS (Sylgard 184 elastomer kit, Dow Corning), the silicone and the curing agent, were mixed together according to the proportion (10:1) for the device layer and with a proportion of (5:1) for the bulk cover layer. After the degassing, the PDMS was poured in the master and placed in oven at 50 °C for 24 h. Finally, the PDMS device was peeled from the master and assembled with a 0.5 mm thick bulk by a reversible bound procedure.

Two PDMS devices were realized: $Device_{400}$ related to the CAD_{400} and the $Device_{200}$ associated to CAD_{200}. In Fig. 9 for the $Device_{400}$, a digital microscope zoom of the area with the micro-channel test section and the three optical fiber insertions and a scanning electron microscope (SEM) image in the area closer to test section are shown.

3 Experimental results and discussion

Two experimental tests were carried out: the first, considering one fluid flowing inside the channel, for the device's static characterization, and the second, for the device's dynamic characterization, by generating a two-phase flow. The comparison of the performance obtained with $Device_{400}$ and $Device_{200}$ is presented.

A global representation of experimental setup considered for the characterization of the devices is shown in Fig. 10a. A picture of the micro-optofluidic device connected with the three optical fibers and the inlet and outlet tubing is in Fig. 10b. Three multi-mode optical fibers with a N.A. = 0.22 (SMA to free end, by Thorlabs) were used
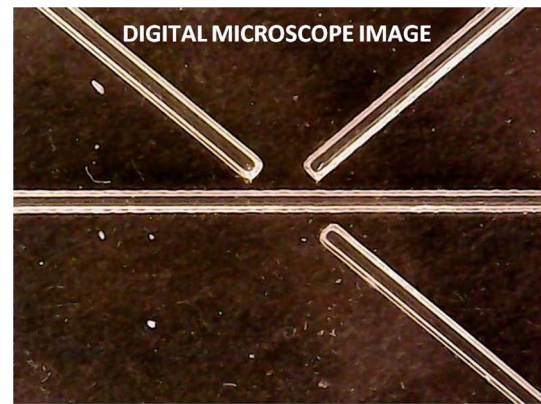
(a)
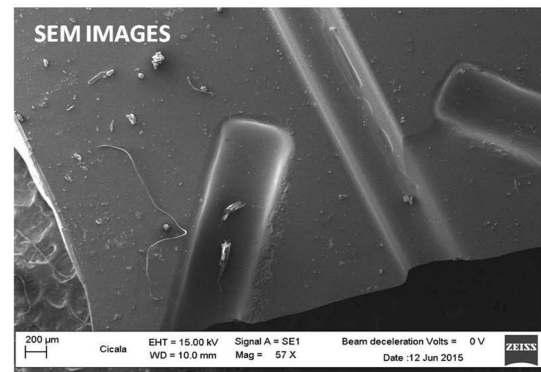
(b)

Fig. 9 PDMS $Device_{400}$. **a** The digital microscope image of the area with the micro-channel and the three optical fiber insertions, **b** a SEM image in the area closer to the test section

and the core diameter, according to the device design, was of 365 µm for $Device_{400}$ and of 200 µm for $Device_{200}$ (see Table 2).

To enlighten the micro-channel test section, in both experiments the free end of the optical fiber was clamped onto the device's input fiber insertion while the SMA-end was connected to the laser source (Rgb NovaPro Laser 660-125) with a wavelength of 660 nm and an output power of 1 mW. The same setup was realized for the other two optical fibers: the free ends clamped onto the output optical fiber insertions (OF_1 or OF_2) and the SMA-ends connected to the detectors.

A pair of syringe pumps (neMESYS by Centoni Gmbh) was used to generate a controlled flow into the micro-channel. For a visual inspection of the process, a digital USB microscope with a direct illumination was placed above the micro-optofluidic device.

3.1 Static characterization

A constant single-phase flow of air or de-ionized water was pumped into the micro-channel with an input flow rate of 0.01 ml min.
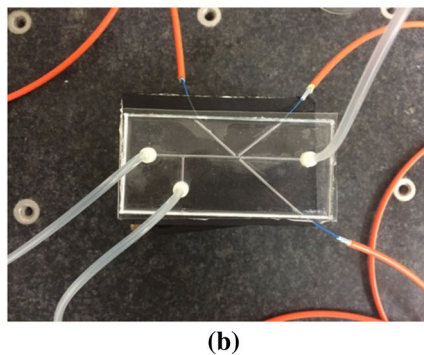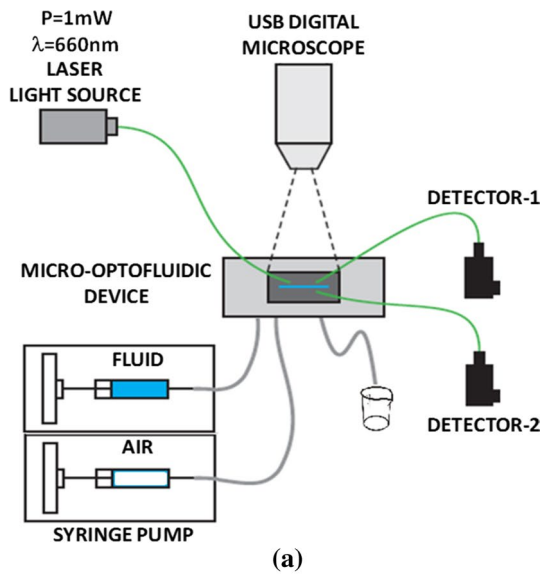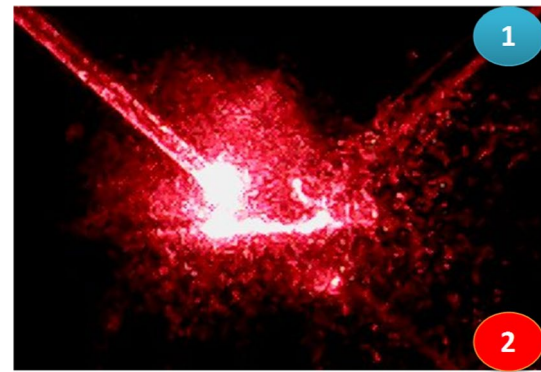
(a)

(b)

Fig. 10 **a** A global representation of experimental setup realized for the device characterization. **b** The picture of the micro-optofluidic device connected with the three optical fibers and the inlet and outlet tubing

(a)

(b)

Fig. 11 The pictures acquired by the digital microscope related to the air passage (*above*) and water passage (*below*) during the static characterization. **a** The micro-channel is filled by air and the larger amount of light is reflected and detected by OF_1. **b** The micro-channel is filled by water and the larger amount of light is transmitted and by OF_2
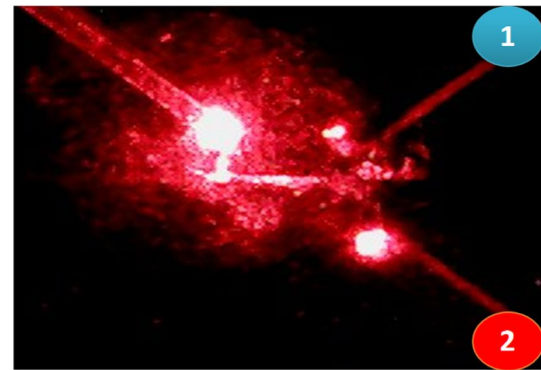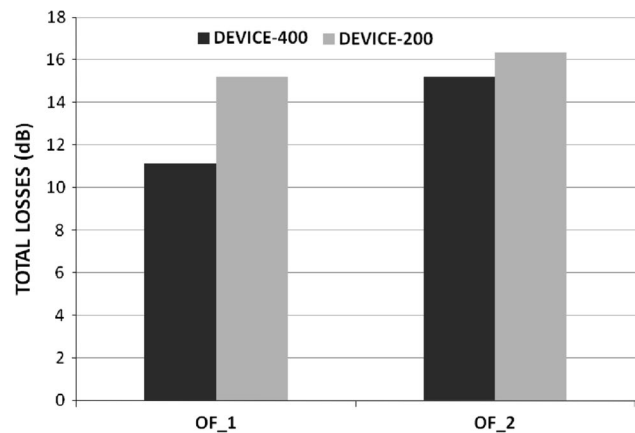
One output fiber was used at a time and connected with a power meter (PM3 by Coherent) to detect the light reflected at the air passage by the insertion OF_1, or the light transmitted at the water passage by the insertion OF_2, respectively.

In Fig. 11 two pictures related to the air passage and water passage acquired by the digital microscope are shown. As it is possible to observe, when the micro-channel is filled with air the larger amount of light is reflected and detected by the output fiber OF_1 in spite of the lower power being directed toward the output fiber OF_2. Conversely, when the micro-channel is filled with water the higher power is detected by the output fiber OF_2.

For both Device$_{400}$ and Device$_{200}$ the total power losses in the reflection condition toward the fiber OF_1 at the air passage and in the transmission condition toward the fiber OF_2 at the water passage, in relation to the power of the laser beam generated at the input, are reported in the bar-plot of Fig. 12. The losses for the Device$_{400}$ are

Fig. 12 The comparison of power total losses in dB, for the Device$_{400}$ and the Device$_{200}$, in the reflection condition toward the fiber OF_1 at the air passage and in the transmission condition toward the fiber OF_2 at the water passage

around 4 % higher in transmission at the water passage than in reflection at the air passage, consistently with the results in simulation. This difference is no more evident

for Device$_{200}$, which has an equal performance in both conditions but worse than the one of Device$_{400}$. This performance worsening is due to the fiber N.A., as in simulations, and additionally, it could be caused by some impurity related to the Sokalan salt of the order of 10 μm still present in the device (see Fig. 9b), introducing a diffuse light scattering dominant at lower dimensions. The residual light power (see Fig. 11), that reaches the other optical fiber in both conditions, is of the order of some μW in OF$_2$ at the air passage and one order less at the water passage.

3.2 Dynamic characterization

The two-phase flow was generated at the micro-channel T-junction by pumping both air and de-ionized water with a constant flow rate of 0.01 ml min. The two output optical fibers were connected to two photodetectors (PDA100A by Thorlabs) coupled with a digital oscilloscope (MSO7054A by Agilent, sampling frequency of 500 Hz) for a continuous and simultaneous monitoring of the light signals both reflected (OF$_1$) and transmitted (OF$_2$).

An initial characterization of the single-phase flow, pumping only air or DI water into the micro-channel, was performed. The mean voltage values of the signals acquired in the case of air passage at the fiber OF$_1$ and in the case of the water passage at fiber OF$_2$ are, for Device$_{400}$ {0.785 and 2.73} V and for Device$_{200}$ {0.47 and 2.08} V. The residual voltage (see Fig. 13) due to the light that reaches the other optical fiber in both conditions is of the order of 10^{-1} V. In the output fiber OF$_1$ the signal is higher at the air presence (in the reflection condition) while in the output fiber OF$_2$ the signal is higher at the water presence (in the transmission condition).

During the continuous two-phase flow generation, the square wave trend of the signals detected at both output fibers reflects the air–water segmented flow in the micro-channel as shown in Fig. 13 for the Device$_{200}$ and the Device$_{400}$. A faster flow with smaller slugs is detected in Device$_{400}$ since the micro-channel diameter is greater.

The dynamic characterization of the switching process and its repeatability was proved by comparing the results obtained for Device$_{400}$, in the other two flow conditions. Meanwhile in the initial experiment (labelled following experiment-1) the fluids used were the DI water and air, in the second experiment (labelled following experiment-2) the DI water was substituted by the Hexadecane (Sigma-Aldrich) with oil-soluble surfactant Span 80 (Sigma-Aldrich) at 2 wt%. As its refractive index ($N_{Hx} = 1.434$) is close to that of the DI water, in the device realization the only parameter modified was the displacement of the output fiber (d). In experiment-3 the fluids used were again DI water and air but the surface of the micro-channel was previously applied with Hexadecane (Sigma-Aldrich) and oil-soluble surfactant Span 80 (Sigma-Aldrich) at 2 wt%.

For both optical fibers (OF$_1$ and OF$_2$) the mean of the switching time was computed, taking into account the ON–OFF and OFF–ON passages, as reported in Table 3. The ON–OFF and the OFF–ON switches occur at the air–fluid
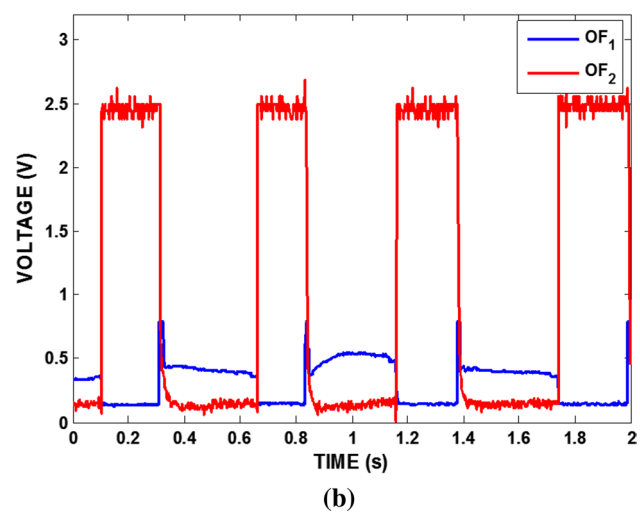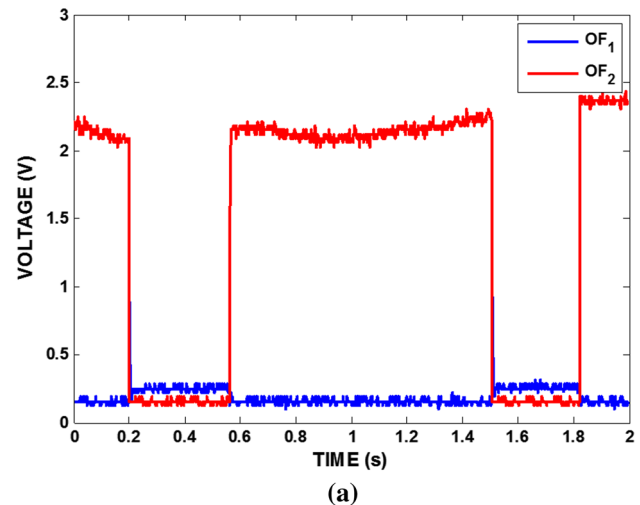

Fig. 13 The square wave trend detected during the continuous two-phase flow generation at both output fibers reflects the air–water segmented flow in the micro-channel. **a** Device$_{200}$ and **b** Device$_{400}$

Table 3 The mean of the switching time in ms considering the ON–OFF and OFF–ON passages, for both output fibers OF$_1$ and OF$_2$

	OF$_1$		OF$_2$	
	Air–fluid (ON–OFF)	Fluid–air (OFF–ON)	Air–fluid (ON–OFF)	Fluid–air (OFF–ON)
Experiment-1	6	18	4	20
Experiment-2	8	10	8	8
Experiment-3	6	6	6	6

and fluid–air passages for the OF_1, and vice-versa for the OF_2. It is possible to observe that the best conditions were obtained in experiment-3, where the use of water leads to a faster switching time of 6 ms and the moistened walls inside the micro-channel stabilizes the transition process keeping its value constant at both passages.

4 Conclusions

The PDMS micro-optofluidic switch presented in this paper consists of a T-junction and three optical fiber insertions realized by 3D printing technology. It allows a two-phase flow to be detected as well as an input laser beam to be steered. A two-phase flow was generated at the T-junction by two streams of air and a second fluid (water or oil). When the laser beam interacts with the microfluidic flow, depending on the fluid in the channel and the laser beam angle of incidence, a different signal level is detected. So a continuous air-fluid segmented flow will generate a signal that switches between two values.

This device can be considered an evolution respect to the standard chip being several aspects related to the use of optical techniques to interfere with a microfluidic flow embedded all together. In literature the laser light is used to control the displacement and the detection of the bubbles, the design of this chip is conceived in a way to be easily adaptable to both uses without the need of any external optic components. It is important to underline: the simplicity of the design, no lenses and mirrors were necessary to obtain satisfactory results, using the simplicity of 3D technology. The master of the device was fabricated by low-cost 3D printing technology and a protocol for the realization of the PDMS chip is presented. Although, up to now, 3D printed structures cannot compete with the resolution of those obtained by the soft-lithography, satisfactory results are shown in both the static and dynamic characterizations with a micro-channel width of up to 200 μm. The sensitivity of the system to capture changes at the flow passage was enhanced by applying the chip wall with hexadecane plus span 80.

For a smaller diameter, as expected from simulations, the introduction of micro-lenses would be necessary for a light beam enhancement and losses reduction. As it can be noticed in the SEM picture of the CAD_{400} (see Fig. 10) some residual Sokalan crystals on the PDMS surface create a light diffusion. Indeed in relation to the high level of precision required in the realization of micro-lenses an improvement in the protocol will be studied.

Thanks to the simplicity in terms of the design and the low production cost, the micro-optofluidic chips realized by 3D technology could represent an important step ahead in the realization of devices with an higher level of functional complexity.

References

Baroud CN, De Saint Vincent MR, Delville JP (2007) An optical toolbox for control of droplet microfluidics. Lab Chip 7:1029–1033

Baroud CN, Delville JP, Gallaire F, Wunenburger R (2007) Thermocapillary valve for droplet production and sorting. Phys Rev E 75:046302

Camou S, Fujita H, Fujii T (2003) PDMS 2D optical lens integrated with microfluidic channels: principle and characterization. Lab Chip 3:40–45

Chang-Yen DA, Eich RK, Gale BK (2005) A monolithic PDMS waveguide system fabricated using soft-lithography techniques. J Lightwave Technol 23:2088–2093

Chan HN, Chen Y, Shu Y, Chen Y, Tian Q, Wu H (2015) Direct, one step molding of 3D printed structures for convenient fabrication of truly 3D PDMS microfluidic chips. Microfluids Nanofluids 19:9–18

Hwanga Y, Paydarb OH, Candlera RN (2015) 3D printed molds for non-planar PDMS microfluidic channels. Sens Actuators A 226:137–142

Lapsley MI, Lin SS, Mao X, Huang TJ (2009) An in-plane, variable optical attenuator using a fluid-based tunable reflective interface. Appl Phys Lett 95:083507

Llobera A, Demming S, Wilke R, Buttgenbach S (2007) Multiple internal reflection poly(dimethylsiloxane) systems for optical sensing. Lab Chip 7:1560–1566

Llobera A, Wilke R, Buttgenbach S (2008) Enhancement of the response of poly(dimethylsiloxane) hollow prisms through air mirrors for absorbance-based sensing. Talanta 75:473–479

McDonald JC, Whitesides GM (2002) Poly(dimethylsiloxane) as a material for fabricating microfluidic devices. Acc Chem Res 35(7):491–499

Ng JM, Gitlin I, Stroock AD, Whitesides GM (2007) Components for integrated poly(dimethylsiloxane) microfluidic systems. Electrophoresis 23:3461–3473

Ono K, Kaneda S, Camou S, Fujii T (2003)Integration of multi-aspherical lenses and optical fibers onto a PDMS microfluidic device for fluorence-based detection. In: 7th International conference on miniaturized chemical and biochemical analysis systems, pp 1307–1310

Song W, Psaltis D (2011) Pneumaticcaly tunable optofluidic 2×2 switch for reconfigurable optical circuit. Lab Chip 11:2397–2402

Rossetto N, Ferrante C (2014) A microfluidic optical beam steerer. Microfluids Nanofluids 16:47–53

Sapuppo F, Bucolo M, Intaglietta M, Johnson PC, Fortuna L, Arena P (2007) An improved instrument for real-time measurement of blood velocity in microvessels. IEEE Trans Instrum Meas 56(6):2663–2671

Sapuppo F, Llobera A, Schembri F, Intaglietta M, Cadarso VJ, Bucolo M (2010) A polymeric micro-optical interface for flow monitoring in bio-microfluidics. Biomicrofluidics 4(1):1–13

Schembri F, Bucolo M (2011) Periodic input flow tuning nonlinear two-phase dynamics. Microfluidics Nanofluidics 11:189–197

Sapuppo F, Schembri F, Fortuna L, Llobera A, Bucolo M (2012) A polymeric micro-optical system for the spatial monitoring in two-phase microfluidics. Microfluidics Nanofluidics 12:165–174

Tabeling P (2005) Introduction to microfluidics. Oxford University Press, Oxford

Van Steijn V, Kreutzer MT, Kleijn CR (2007) PIV study of the formation of the segmented flow in microfluidic T-junction. Chem Eng Sci 62:7505–7514

Weber E, Keplinger F, Vellekoop MJ (2012) Detection of dissolved lactose employing an optofluidic micro-system. Diagnostics 2:97–106

Whitesides GM (2006) The origins and the future of microfluidics. Nature 442:368–373

Yeshaiahu F, Lee LP, Psaltis D, Yang C (2010) Optofluidics fundamentals, devices, and application. McGraw-Hill, New York